Cai *et al. BMC Cancer* (2025) 25:461
https://doi.org/10.1186/s12885-025-13804-x

BMC Cancer

RESEARCH Open Access

Integration of intratumoral and peritumoral CT radiomic features with machine learning algorithms for predicting induction therapy response in locally advanced non-small cell lung cancer

FangHao Cai[1,3†], Zhengjun Guo[1,3*†], GuoYu Wang[2], FuPing Luo[2], Yang Yang[2], Min Lv[2], JiMin He[2], ZhiGang Xiu[2], Dan Tang[2], XiaoHui Bao[1,3], XiaoYue Zhang[1,3], ZhenZhou Yang[1,3*] and Zhi Chen[2,1*]

Abstract

Objectives To extract intratumoral, peritumoral, and integrated intratumoral-peritumoral CT radiomic features, develop multi-source radiomic models using various machine learning algorithms to identify the optimal model, and integrate clinical factors to establish a nomogram for predicting the therapeutic response to induction therapy(IT) in locally advanced non-small cell lung cancer.

Methods This study included 209 patients with locally advanced non-small cell lung cancer (LA-NSCLC) who received IT as the training cohort, and an external validation cohort comprising 50 patients from another center. Radiomic features were extracted from intratumoral, peritumoral, and integrated intratumoral-peritumoral regions by manually delineating the gross tumor volume (GTV) and an additional 3 mm surrounding area. Three machine learning algorithms—Support Vector Machine (SVM), XGBoost, and Gradient Boosting—were employed to construct radiomic models for each region. Model performance was evaluated in the external validation cohort using metrics such as Area Under the Curve (AUC), confusion matrix, accuracy, precision, recall, and F1 score. Finally, a comprehensive nomogram integrating the optimal radiomic model with independent clinical predictors was developed.

Results Through a comparison of optimal machine learning algorithms, INTRAPERI, INTRA, and PERI achieved the best performance with Gradient Boosting, SVM, and XGBoost, respectively. Compared to the INTRA_SVM and

†FangHao Cai and Zhengjun Guo contributed equally to the work.

*Correspondence:
Zhengjun Guo
guozhengjun@hospital.cqmu.edu.cn
ZhenZhou Yang
yangzz@cqmu.edu.cn
Zhi Chen
2023440076@stu.cqmu.edu.cn

Full list of author information is available at the end of the article

PERI_XGBoost INTRA models, the fusion model that integrates INTRA and peritumoral regions within a 3 mm margin around the tumor (INTRAPERI_GradientBoosting) showed better predictive performance in the training set, with AUCs of 93.7%, 82.5%, and 89.4%, respectively. In the clinical model, the PS score was identified as an independent predictive factor. The nomogram combining clinical factors with the INTRAPERI_GradientBoosting score demonstrated clinical predictive value.

Conclusion The INTRAPERI_GradientBoosting model, which integrates intra-tumoral and peritumoral features, performs better than the INTRA intra-tumoral and PERI peritumoral radiomics models in predicting the efficacy of IT therapy in LA-NSCLC. Additionally, the nomogram based on INTRAPERI intra-tumoral and peritumoral features combined with independent clinical predictors has clinical predictive value.

Keywords Radiomics, Non-small cell lung cancer (NSCLC), Locally advanced, Induction therapy, Machine learning, CT imaging, Intra-tumoral features, Peritumoral features, Predictive model, Nomogram

Introduction

Lung cancer is the most prevalent malignant tumor worldwide, with non-small cell lung cancer (NSCLC) accounting for 80-85% of cases [1]. At diagnosis, approximately 25% of NSCLC patients present with locally advanced disease (Locally Advanced Non-Small Cell Lung Cancer, LA-NSCLC), characterized by local tissue and lymph node metastases without distant organ involvement. These patients still have the potential for clinical cure [2].

In clinical practice, LA-NSCLC often exhibits poor treatment outcomes and reduced survival due to tumor local invasion and metastasis [3]. Although IT, including chemotherapy, radiotherapy, targeted therapy, and immunotherapy, aims to eliminate micrometastases and reduce tumor burden, thereby improving prognosis for some patients, the 5-year survival rate remains between 10 and 30% [4–6]. Accurately assessing the efficacy of IT for LA-NSCLC remains a significant clinical challenge. Therefore, identifying effective biomarkers and radiomic features is crucial for enhancing clinical efficacy evaluation and personalized treatment.

The metastatic process of LA-NSCLC is complex, involving tumor cell invasion of microvasculature and lymphatics, directly representing its metastatic progression [7, 8]. Studies indicate that the tumor's internal microvasculature is often occluded by tumor and stromal cells, potentially leading to functional loss, making it unclear if INTRA (intra-tumoral) conditions accurately reflect hematogenous metastasis [9, 10]. In contrast, peripheral blood vessels generally remain functional, and their infiltration may facilitate distant metastasis [11]. The microenvironment differences within and around the tumor in LA-NSCLC are closely linked to metastasis, treatment outcomes, and patient survival.

Radiomics, which integrates traditional medical imaging with machine learning (ML) algorithms for predictive analysis, has emerged as an auxiliary tool in oncology. Research shows that CT imaging can not only clearly delineate tumor boundaries from normal lung parenchyma but also reveal attenuation transition zones at these boundaries [12]. Concurrently, ML algorithms effectively identify patterns in data, characterizing the heterogeneous features inside and outside the tumor, thereby enhancing prediction accuracy and reliability [13].

Although previous studies have explored radiomics applications in INTRA and peritumoral features, real-world research specific to LA-NSCLC remains limited. This study focuses on LA-NSCLC with the aim of developing and validating ML models based on peritumoral, INTRA, and combined features to predict the efficacy of IT in LA-NSCLC, thereby establishing stable and accurate predictive models for newly diagnosed LA-NSCLC patients.

Materials and methods

Study design

This study was designed as a Transparent Reporting of a Multivariable Prediction Model for Individual Prognosis or Diagnosis (TRIPOD) Type 3 study, encompassing model development and independent validation [14]. It was registered on the Biomedical Research Artificial Intelligence Platform (ID: jOis7e) [15]. The overall study workflow is illustrated in Fig. 1.

Patients

This retrospective study was approved by the Institutional Review Board of Sichuan University West China Longquan Hospital (Approval No.: IRB-C-F10/AF-KY-2024028), and the requirement for written informed consent was waived. A total of 209 patients with locally advanced non-small cell lung cancer (LA-NSCLC) who underwent chest contrast-enhanced CT scans and subsequent IT (including chemotherapy, radiotherapy, and immunotherapy) at Sichuan University West China Longquan Hospital between January 2018 and December 2023 were included in the study. Clinical data, chest CT images, and blood-related biomarkers were collected and anonymized for analysis.

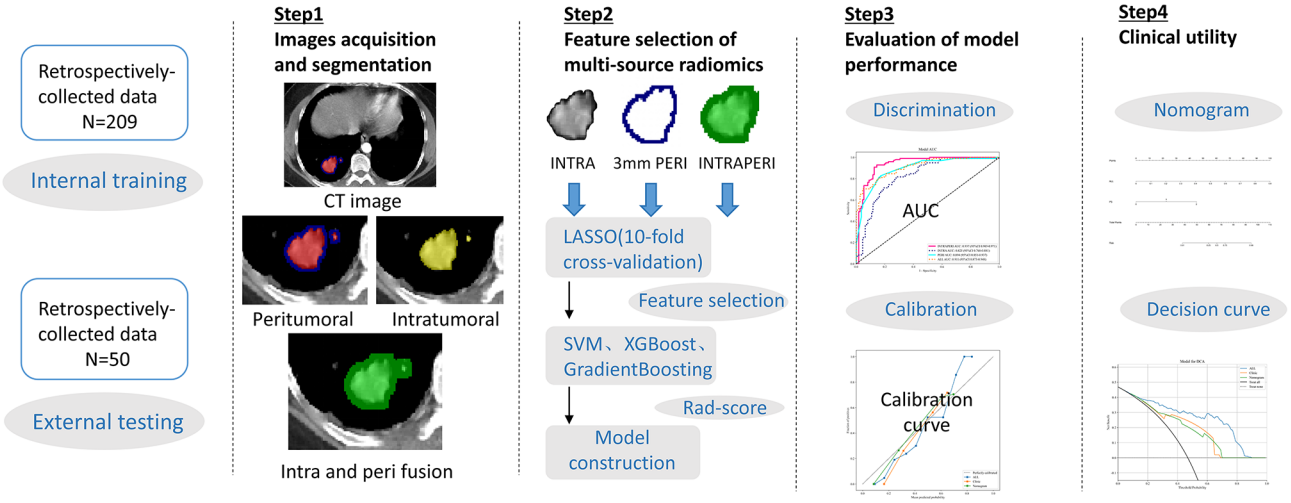

Fig. 1 Analysis Workflow. The workflow consists of the following steps: **Feature Extraction**: Radiomic and dosimetric features are extracted from lung tissue regions. **Feature Selection and Modeling**: Features are extracted and selected from intra-tumoral, 3 mm peritumoral, and fused intra-peritumoral regions using correlation analysis, Least Absolute Shrinkage and Selection Operator (LASSO) regression, and embedded logistic regression with three machine learning classification algorithms. **Model Evaluation**: Model performance is assessed through discrimination and calibration metrics. **Clinical Application Assessment**: The clinical applicability is evaluated using a nomogram and decision curve analysis

This study also included a patient cohort from another institution, the Cancer Center of the Second Affiliated Hospital of Chongqing Medical University, which served as an external validation cohort. These patients were retrospectively enrolled from December 2023 to June 2024, using the same inclusion criteria as the primary cohort. A total of 50 LA-NSCLC patients were identified for inclusion in the external validation cohort.

The enrollment, eligibility, and exclusion criteria for both the training and external validation cohorts are detailed in Fig. 2.

Efficacy assessment was conducted by two senior oncologists and two senior radiologists based on the Response Evaluation Criteria in Solid Tumors (RECIST) version 1.1. By comparing pre- and post-chemotherapy CT images, clinical responses were categorized into four groups: (I) Complete Response (CR): disappearance of all target lesions; (II) Partial Response (PR): at least a 30% reduction in the sum of diameters of target lesions; (III) Progressive Disease (PD): at least a 20% increase in the sum of diameters of target lesions; and (IV) Stable Disease (SD): neither sufficient shrinkage to qualify for PR nor sufficient increase to qualify for PD [16]. Patients achieving PR or CR were defined as "responders," while those with SD or PD were defined as "non-responders." Patient characteristics are listed in Table 1.

Image acquisition

CT Scanning Protocol: All LA-NSCLC patients underwent chest contrast-enhanced CT scans at their respective hospitals before treatment (Supplementary Data).

Image preprocessing and segmentation

Preprocessing: To eliminate confounding factors, CT images were standardized and resampled before feature extraction. Images were normalized by subtracting the window level (WL: -500) and dividing by the window width (WW: 1500), then resampled to a voxel size of $1 \times 1 \times 1$ mm^3.

Two senior radiologists manually delineated the gross tumor volume (GTV) using ITK-SNAP (version 4.2.2, https://www.itksnap.org), defining the INTRA region. The PERI (peritumoral) region was defined as the area extending 3 mm outward from the GTV using a Python 3.1.1 (https://www.python.org) script that applied a 3D dilation algorithm to the tumor area, subtracted the original tumor area, and delineated the 3 mm peritumoral region. Areas adjacent to the chest wall and vertebral bodies were manually excluded by the radiologists.

The INTRAPERI (intra-tumoral and peritumoral fusion) region was obtained by applying a 3D dilation algorithm to create a combined 3 mm fusion area around the tumor, from which radiomic features were extracted.

Radiologists 1 and 2 assessed intra-observer and inter-observer reproducibility using 30 randomly selected chest CT images. An intraclass correlation coefficient (ICC) > 0.75 indicated good consistency.

Radiomic feature extraction and selection

Feature Extraction: Radiomic features were extracted from the regions of interest (ROIs) using the open-source PyRadiomics package (version 3.1.0, https://pyradiomics.readthedocs.io/en/latest/changes.html). A total of 1,835 radiomic features were extracted, including 14 shape features, 360 first-order features, 440 Gy level

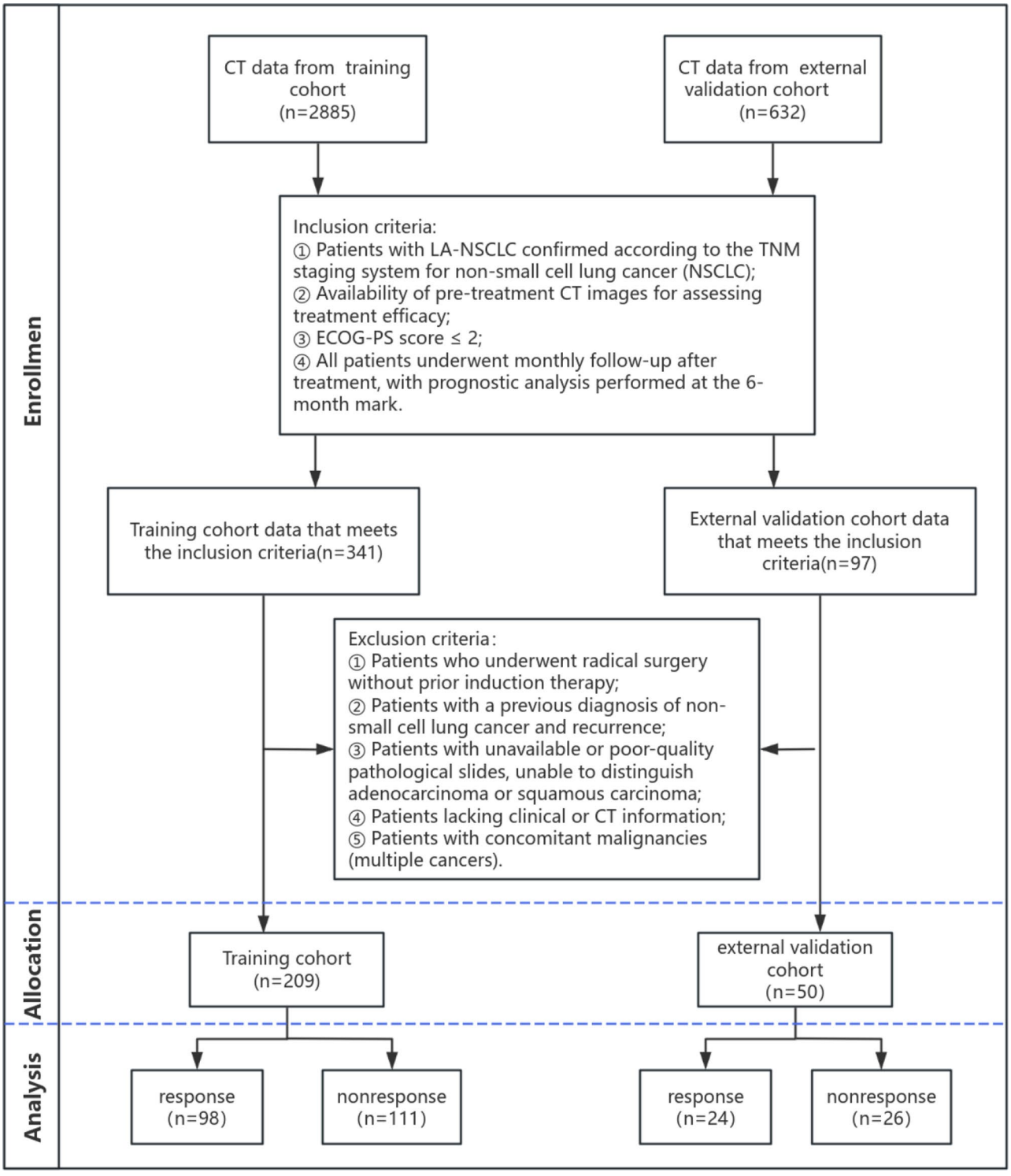

Fig. 2 Flowchart of patient enrollment, eligibility, and exclusion criteria

co-occurrence matrix (GLCM) features, 320 Gy level run length matrix (GLRLM) features, 320 Gy level size zone matrix (GLSZM) features, 280 Gy level dependence matrix (GLDM) features, and 100 neighborhood gray tone difference matrix (NGTDM) features, following the Image Biomarker Standardisation Initiative (IBSI) guidelines [17].

Feature Standardization: The extracted features were standardized using the Z-score method, as the images were acquired from different scanners with varying

Table 1 Baseline characteristics of patients in cohorts

Characteristics		Training cohort ($n=209$)			Validation cohort ($n=50$)			*p*
		noresponse ($n=111$)	Response ($n=98$)	*p*	noresponse ($n=26$)	response ($n=24$)	*p*	
Age		64.41 ± 9.15	62.89 ± 8.69	0.222	64.40 ± 8.46	63.76 ± 6.97	0.772	0.289
Gender	male	75(67.57)	81(82.65)	0.019	21(84.00)	22(88.00)	1	0.11
	female	36(32.43)	17(17.35)		4(16.00)	3(12.00)		
Histopathology	Adenocarcinoma	66(59.46)	50(51.02)	0.278	14(56.00)	9(36.00)	0.256	0.756
	Squamous Cell Carcinoma	45(40.54)	48(48.98)		11(44.00)	16(64.00)		
Tx	0	3(2.70)	2(2.04)	0.189	1(4.00)	2(8.00)	0.675	0.398
	1	14(12.61)	20(20.41)		6(24.00)	3(12.00)		
	2	57(51.35)	37(37.76)		9(36.00)	9(36.00)		
	3	37(33.33)	39(39.80)		9(36.00)	11(44.00)		
Nx	0	9(8.11)	5(5.10)	< 0.001	2(8.00)	1(4.00)	0.349	0.076
	1	8(7.21)	8(8.16)		1(4.00)	4(16.00)		
	2	24(21.62)	59(60.20)		10(40.00)	6(24.00)		
	3	70(63.06)	26(26.53)		12(48.00)	14(56.00)		
Overall_Stage	IIIa	27(24.32)	22(22.45)	< 0.001	4(16.00)	5(20.00)	0.519	0.003
	IIIb	21(18.92)	64(65.31)		13(52.00)	9(36.00)		
	IIIc	63(56.76)	12(12.24)		8(32.00)	11(44.00)		
ECOG-PS	0	32(28.83)	71(72.45)	< 0.001	9(36.00)	18(72.00)	0.032	< 0.001
	1	64(57.66)	27(27.55)		15(60.00)	7(28.00)		
	2	15(13.51)	null		1(4.00)	null		
Smoking	Never	57(51.35)	36(36.73)	0.074	8(32.00)	4(16.00)	0.276	0.657
	Quit	42(37.84)	52(53.06)		17(68.00)	20(80.00)		
	Currently Smoking	12(10.81)	10(10.20)		null	1(4.00)		
Diabetes	No	92(82.88)	82(83.67)	1	22(88.00)	21(84.00)	1	0.613
	Yes	19(17.12)	16(16.33)		3(12.00)	4(16.00)		
COPD	No	81(72.97)	63(64.29)	0.229	15(60.00)	8(32.00)	0.089	0.613
	Yes	30(27.03)	35(35.71)		10(40.00)	17(68.00)		
Tumor_Location	Left	40(36.04)	43(43.88)	0.31	14(56.00)	11(44.00)	0.572	0.155
	Right	71(63.96)	55(56.12)		11(44.00)	14(56.00)		
Lung_Lobe	Upper	55(49.55)	33(33.67)	0.037	17(68.00)	15(60.00)	0.203	0.33
	Middle	14(12.61)	11(11.22)		null	3(12.00)		
	Lower	42(37.84)	54(55.10)		8(32.00)	7(28.00)		
Chemotherapy	No	15(13.51)	11(11.22)	0.772	11(44.00)	3(12.00)	0.027	0.506
	Yes	96(86.49)	87(88.78)		14(56.00)	22(88.00)		
Immunotherapy	No	69(62.16)	49(50.00)	0.103	16(64.00)	7(28.00)	0.023	0.464
	Yes	42(37.84)	49(50.00)		9(36.00)	18(72.00)		
Radiotherapy	No	31(27.93)	44(44.90)	0.016	16(64.00)	6(24.00)	0.01	0.0256
	Yes	80(72.07)	54(55.10)		9(36.00)	19(76.00)		

imaging protocols. Both training and validation datasets were normalized using min–max scaling, where each feature was scaled to a range from 0 to 1.

$$Z\ \text{score} = \frac{(x - \mu)}{\sigma}$$

Here, χ represents the value of the feature, μ\muμ denotes the mean of that feature across all patients in the cohort, and σ\sigmaσ indicates the corresponding standard deviation [18].

Feature Selection: Initially, Mann-Whitney U tests were performed, retaining features with p-values < 0.05. Subsequently, Spearman correlation analysis was conducted to eliminate highly correlated features (correlation coefficient > 0.9) [19]. Finally, the Least Absolute Shrinkage and Selection Operator (LASSO) was applied with 10-fold cross-validation to further select the most predictive features while minimizing overfitting, resulting in the final set of radiomic features [20].

Construction of radiomic models

Radiomic Score: Three machine learning classification algorithms—Support Vector Machine (SVM), XGBoost, and Gradient Boosting—were used to build radiomic models based on the selected features. The best-performing models for INTRAPERI, INTRA, and PERI were identified as INTRAPERI_GradientBoosting, INTRA_SVM, and PERI_XGBoost, respectively. Radiomic scores (Rad-scores) were calculated as weighted linear combinations of the selected features:

$$\text{Radiomic signature(Rad - score)} = \sum {}_{i=1}^{n} C_i X_i + b$$

where b is the intercept, is the value of ith selected feature and is the coefficient of the i th selected feature [21].

The optimal radiomic models were trained and validated using 5-fold cross-validation on the training cohort, and their performance was subsequently evaluated in the external validation cohort.

Selection of Clinical Parameters: Clinical factors with statistical significance in univariate analysis were included in a multivariate logistic regression to identify independent predictors of response to IT.

Construction and Validation of the Nomogram: A comprehensive nomogram was developed by combining the optimal radiomic model with independent clinical predictors. Its predictive performance was evaluated in both internal and external validation cohorts using ROC curves, calibration curves (assessed by Hosmer-Lemeshow tests), and decision curve analysis (DCA) to determine clinical utility.

Statistical analysis

All statistical analyses were performed using R software (version 4.2.2). Continuous variables were compared using independent samples Student's t-test or Wilcoxon Mann-Whitney U test as appropriate, and categorical variables were compared using chi-square tests or Fisher's exact tests when necessary. Univariate and multivariate logistic regression analyses were conducted to identify predictors of response to IT in LA-NSCLC. Spearman correlation was used to remove redundant high-dimensional features. LASSO logistic regression was performed using the "glmnet" package in R. The "rms" package was used to construct the nomogram and calibration curves, with the Hosmer-Lemeshow test evaluating model fit [22]. ROC curves and AUC values were used to assess discriminative performance, and DeLong's test was applied to compare AUCs between models to evaluate overfitting. Decision curve analysis was conducted to evaluate the clinical benefit of the models [23]. Supplementary Figs. 2 and 3, and Supplementary Table 4 provide additional details on model performance and calibration.

Results

Clinical characteristics

A total of 259 patients were included in this study, with 209 in the training cohort and 50 in the external validation cohort. After IT, clinical efficacy was evaluated based on the Response Evaluation Criteria in Solid Tumors (RECIST) version 1.1. In the training cohort, 98 patients were responders (46.88% ORR: SD 99, CR 7, PR 91, PD 12), and in the external validation cohort, 24 patients were responders (48% ORR: SD 25, CR 1, PR 23, PD 1). The clinical characteristics of the patients are presented in Table 1.

Univariate analysis revealed that PS score, gender, stage (Overall_Stage), and radiotherapy were significantly associated with the efficacy of IT in LA-NSCLC. These four clinical parameters were included in a multivariate logistic regression analysis, which identified the PS score as an independent predictor of therapy response ($p < 0.05$), as shown in Table 2. This parameter was subsequently used to construct the combined model.

Table 2. Univariate and Multivariate Logistic Regression Analysis of Factors in the Training Cohort.

Construction of radiomic models

Feature selection

Radiomic features were extracted from the regions of interest (ROIs) using the open-source PyRadiomics package. A total of 1,835 radiomic features were obtained for the INTRA, PERI, and INTRAPERI regions, including 14 shape features, 360 first-order features, 440 Gy level co-occurrence matrix (GLCM) features, 320 Gy level run length matrix (GLRLM) features, 320 Gy level size zone matrix (GLSZM) features, 280 Gy level dependence matrix (GLDM) features, and 100 neighborhood gray tone difference matrix (NGTDM) features.

Table 2 Univariable and multivariable logistic regression analysis of factors in the training cohort

Characteristics	Univariate regression		Multivariate regression	
	OR (95% CI)	p_value	OR (95% CI)	p_value
PS	0.352 (0.251–0.495)	< 0.001	0.290 (0.185–0.453)	< 0.001
Gender	0.472 (0.291–0.766)	0.011	0.576 (0.32–1.036)	0.122
Radiotherapy	0.675 (0.505–0.902)	0.026	1.446 (0.918–2.28)	0.183
Overall_Stage	0.730 (0.613–0.869)	0.003	1.066 (0.806–1.411)	0.708

OR Odds Ratio, CI Confidence Interval

To reduce overfitting and selection bias, a series of dimensionality reduction and feature selection methods were applied prior to modeling:

1. Mann-Whitney U Test and Feature Filtering: Features with p-values < 0.05 were retained, resulting in 645, 548, and 588 features for INTRA, PERI, and INTRAPERI, respectively.
2. Spearman Correlation Analysis: Highly correlated features (correlation coefficient > 0.9) were removed, leaving 71, 96, and 76 features for INTRA, PERI, and INTRAPERI, respectively.
3. LASSO Regression: Least Absolute Shrinkage and Selection Operator (LASSO) regression with 10-fold cross-validation was used to further select the most predictive features, resulting in 15, 7, and 13 features for INTRAPERI, INTRA, and PERI radiomic models, respectiFig. (Fig. 3). Additional penalized feature selection for INTRA, PERI, and INTRAPERI is shown in Supplementary Figure S1.

Performance of radiomic features

Optimal radiomic models for each ROI were constructed using three machine learning algorithms: Gradient Boosting, Support Vector Machine (SVM), and XGBoost. The performance of these models was evaluated using accuracy (ACC), sensitivity (SEN), specificity (SPE), positive predictive value (PPV), negative predictive value (NPV), and area under the curve (AUC) in both training and testing datasets. The best-performing models were identified as INTRAPERI_GradientBoosting, INTRA_SVM, and PERI_XGBoost.

Notably, the AUCs for the fusion models (INTRAPERI) were higher than those for the corresponding INTRA or peritumoral models in both training and external validation cohorts. Specifically, in the training cohort, the AUCs were 0.937 for INTRAPERI_GradientBoosting, 0.83 for INTRA_SVM, and 0.894 for PERI_XGBoost. In the external validation cohort, the AUCs were 0.797, 0.734, and 0.76, respectively.Comparison of different region models indicated that the 3 mm fusion region model had the best predictive performance (see Supplementary Tables S1–S3 for detailed performance metrics of the INTRAPERI, INTRA, and PERI region models).

Regarding model calibration, the INTRAPERI ($P = 0.00001451$), INTRA ($P = 0.0002691$), and PERI ($P = 0.0000003908$) models showed significant calibration bias in the training set. However, in the external validation cohort, the Hosmer-Lemeshow test indicated no significant calibration bias for all models, suggesting balanced predictive performance in independent samples despite initial biases in the training data.

The predictive performance of radiomic features, clinical parameters, and the comprehensive nomogram in both training and validation cohorts, along with decision curve analysis, are detailed in Supplementary Figures S2 and S3. The p-values for decision curve analysis are

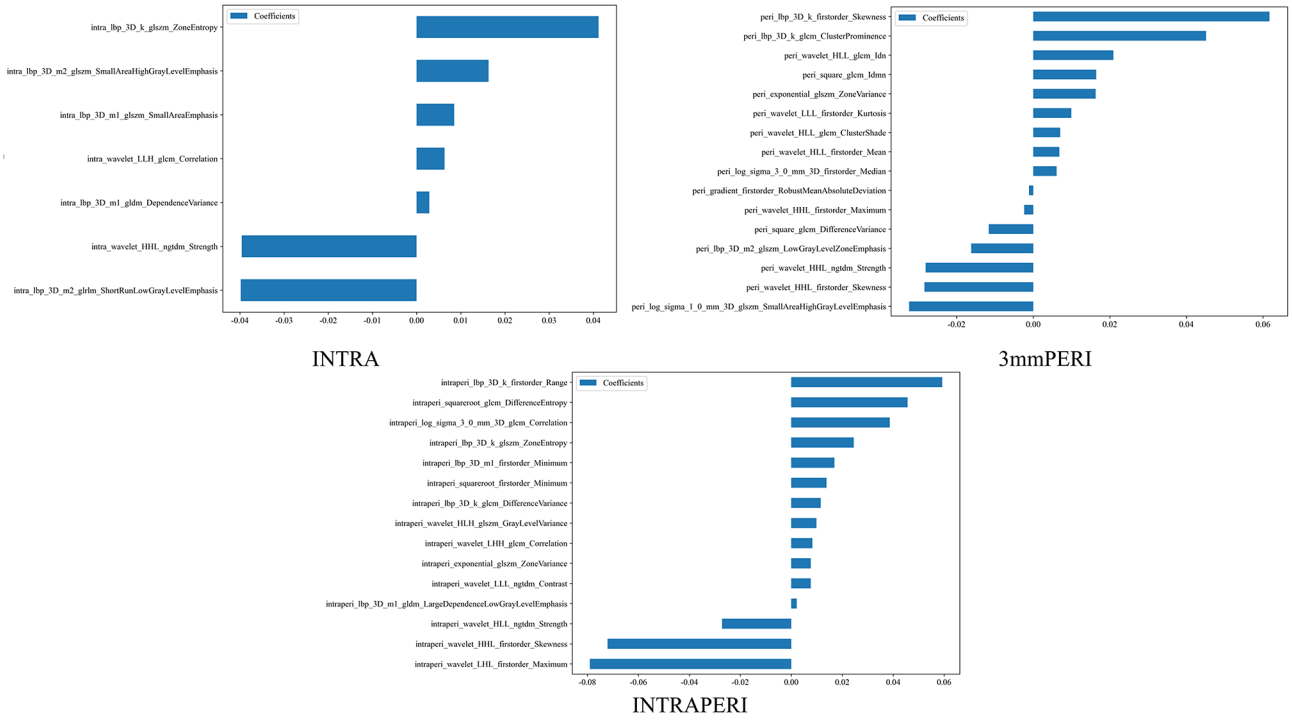

Fig. 3 Coefficients for feature selection in fused intra-peritumoral, intra-tumoral, and peritumoral regions

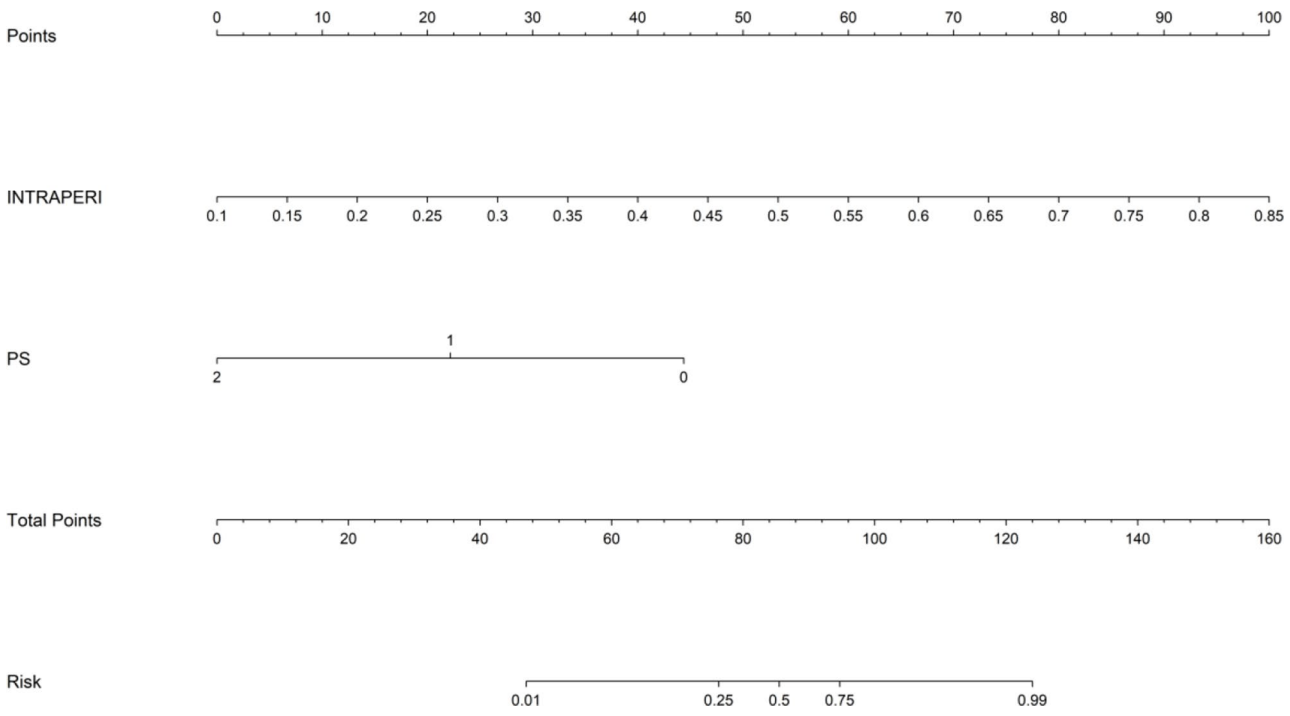

Fig. 4 Nomogram of the comprehensive predictive model combining the 3 mm peritumoral-fused intra-peritumoral feature model with clinical predictive factors

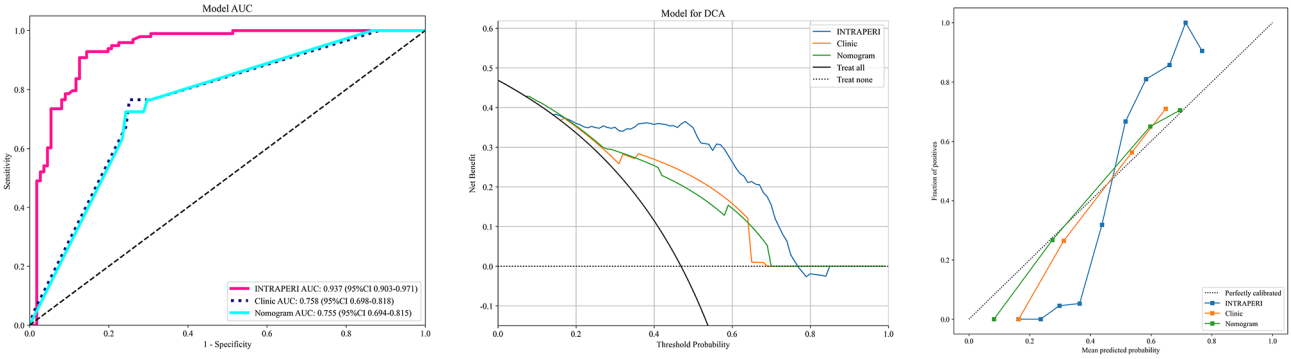

Fig. 5 Predictive performance of the final model's radiomic features, clinical parameters, and comprehensive nomogram in the training cohort. decision curve analysis and calibration curves

derived from the Hosmer-Lemeshow test (see Supplementary Table S4 for detailed results).

Performance and validation of the comprehensive nomogram

A comprehensive predictive model was developed by combining the 3 mm fusion radiomic model with clinical predictors, resulting in a nomogram (Fig. 4) to assess the response to IT in newly diagnosed LA-NSCLC patients.

The performance of the nomogram was evaluated using AUC values:

- Training Cohort: AUC = 0.755 (95% CI: 0.6940–0.8152)(Fig. 5).
- External Validation Cohort: AUC = 0.731 (95% CI: 0.5892–0.8732) (Fig. 6)

The Hosmer-Lemeshow test showed non-significant p-values for both internal validation ($p = 0.358$) and external validation ($p = 0.179$), indicating good calibration. This suggests that the predicted risks by the comprehensive nomogram are well-aligned with the observed outcomes (see Supplementary Table 4). Overall, the comprehensive model demonstrated good performance in the external validation cohort, providing reliable risk prediction and decision support for clinical practice.

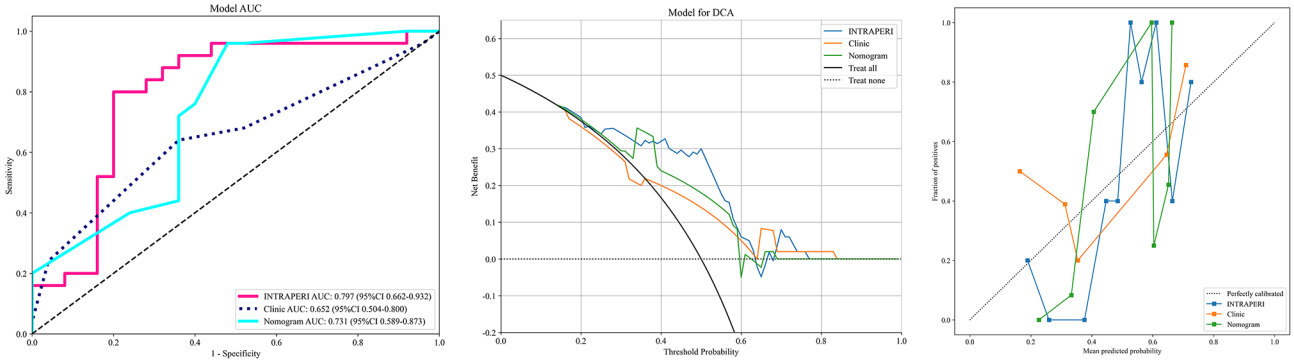

Fig. 6 Predictive performance of radiomic features, clinical parameters, and the comprehensive nomogram in the external validation cohort. Includes decision curve analysis and calibration curves

Discussion

In this multicenter study, we extracted radiomic features from INTRA, peritumoral, and fusion regions of LA-NSCLC using three machine learning (ML) algorithms. The INTRAPERI, INTRA, and PERI models achieved their best predictive performance with Gradient Boosting, SVM, and XGBoost classifiers, respectively. Notably, the INTRAPERI model demonstrated superior predictive capability for IT efficacy compared to the INTRA and PERI models. These findings suggest that peritumoral features effectively reflect IT response, and the fusion of INTRA and peritumoral features provides additional predictive value beyond individual regions.

For feature extraction within INTRA and peritumoral regions, we employed an image fusion method to incrementally obtain radiomic features. In contrast, traditional feature fusion methods typically merge n features from INTRA and peritumoral regions into 2n features, followed by feature selection—a common approach in previous studies [20, 24]. While this method can yield more discriminative features, it may lead to feature redundancy and increased computational burden, potentially overlooking spatial relationships and interactive information between tumor regions.

Conversely, image fusion preserves the unique characteristics of each region and integrates spatial associations, thereby more effectively capturing the heterogeneity of the tumor microenvironment [25]. This approach allows for the extraction of more precise and biologically meaningful features, enhancing the clinical value of disease diagnosis, staging, and treatment efficacy evaluation. Therefore, we believe that image fusion better reflects the spatial heterogeneity of the tumor microenvironment compared to feature fusion, providing a more accurate representation of radiomic features.

Optimal peritumoral region selection

Our results indicate that radiomic features from the 3 mm fusion region around the tumor can predict the IT response in LA-NSCLC. The biological characteristics of lung cancer are not only reflected in the primary tumor but also in the surrounding tissue microenvironment. Combining radiomics with ML methods shows significant potential in predicting clinical treatment responses.

Regarding the selection of the peritumoral region in NSCLC, previous studies have explored multiple scales for segmentation in predicting chemotherapy response [26]. These studies found that radiomic models based on the 0–3 mm peritumoral region outperformed those using 3–6 mm, 6–9 mm, and 9–12 mm regions, achieving the highest AUC of 0.95. By merging features from both the 0–3 mm and 3–6 mm peritumoral regions, the AUC further increased to 0.97. Our findings are consistent with these results. Additionally, previous research [12] indicates that the transition zone between the lung adjacent to cancer (LAC) and normal lung tissue ranges from 1 mm to 5 mm. Based on these considerations, we selected a 3 mm peritumoral region as our ROI.

Selection of optimal ML algorithms for each region

Drawing on our previous meta-analysis on the predictive performance of ML models for radiation-induced pneumonitis in lung cancer, we adopted a similar structure, demonstrating that pretraining multiple ML algorithms can lead to superior models [27]. By comparing the performance of INTRAPERI_GradientBoosting, INTRA_SVM, and PERI_XGBoost, we established our final radiomic models for predicting IT efficacy in LA-NSCLC.

Furthermore, when constructing the radiomic Rad-score, we attempted to integrate the best-performing ML algorithms—INTRAPERI_GradientBoosting, INTRA_SVM, and PERI_XGBoost—into a comprehensive ALL-Rad-score model. This integrated model achieved an impressive AUC of 0.917 in the training cohort (see Supplementary Fig. 2). However, we were concerned that solely merging peritumoral regions might introduce noise and lose heterogeneity information between regions. Consequently, we opted to use only the

INTRAPERI model for the final Rad-score, ensuring high predictive performance while preserving the heterogeneity of INTRA and peritumoral regions. This choice not only optimized prediction but also enhanced the model's clinical applicability and interpretability.

Clinical findings

In our study, responders and non-responders to IT differed significantly in Eastern Cooperative Oncology Group Performance Status (ECOG-PS), gender, stage (Overall_Stage), and receipt of radiotherapy (all $p < 0.05$). Multivariate logistic regression confirmed that ECOG-PS score is an independent predictor of IT response in LA-NSCLC patients ($p < 0.05$), consistent with previous studies [28–30], indicating that ECOG-PS effectively reflects patients' overall health and functional status.

Combining clinical features with radiomic features resulted in a model with an AUC of 0.758 in the training cohort. However, in the external validation cohort, the model using only ECOG-PS scores achieved an AUC of 0.652. This suggests that integrating radiomics with clinical information provides a model with some generalizability. Nonetheless, in the comprehensive nomogram model, adding clinical features did not significantly improve predictive performance in the external validation cohort compared to using radiomic features alone. This implies that although clinical features like ECOG-PS are statistically significant predictors, their contribution to enhancing the overall performance of the radiomics-dominated model is relatively limited.

Implications of radiomic analysis

Our findings demonstrate that quantitative radiomic analysis of the peritumoral region can aid in predicting IT response in LA-NSCLC patients, as the heterogeneity of the tumor microenvironment (e.g., microvasculature, lymphatic invasion, and lymphocyte infiltration) is captured by corresponding radiomic features [12]. The INTRAPERI model, which integrates imaging features from both the tumor and surrounding lung parenchyma, enhances predictive performance and model stability. However, this model primarily focuses on the tumor edge region and may not fully encompass the complex heterogeneity of the entire tumor.

To address this, we attempted to combine radiomic features with clinical information to develop a more comprehensive predictive model, aiming to provide a broader perspective for evaluating IT response in LA-NSCLC patients. Although this approach did not significantly improve predictive performance, incorporating multidimensional information offers a more comprehensive reference for clinical application, supporting personalized treatment decisions and optimization.

Limitations

This study has several limitations. First, while we trained the model using a relatively large CT imaging dataset, the heterogeneity of the data sources may introduce bias, affecting its generalizability. Future studies should validate the model on more diverse datasets to ensure its applicability across different regions and equipment. Second, although radiomic features provide rich information, the complexity of their extraction and analysis limits clinical implementation [31]. Enhancing the interpretability of radiomic models is an important challenge for future research.

Regarding calibration bias, the Hosmer-Lemeshow test on the training set indicated some discrepancies, likely due to overfitting. While LASSO regression mitigates overfitting by regularizing the selection of relevant features, small sample sizes may still lead to overfitting, causing a gap between predicted and actual outcomes [32]. Additionally, local features, noise, and sample imbalances in the training set may exacerbate calibration bias. To improve generalizability, future work will expand the training set and apply advanced bootstrap resampling techniques to reduce overfitting [33].

Lastly, although the model shows promise in predicting treatment response for locally advanced NSCLC, further optimization and validation are needed. Future efforts should explore advanced machine learning and deep learning algorithms, such as CNNs and image enhancement techniques, to improve model performance and robustness [34]. Additionally, integrating molecular biological data and other imaging modalities like PET-CT and MRI will offer a more comprehensive approach to tumor precision treatment [35, 36].

Abbreviations

AUC	Area Under the Curve
CNN	Convolutional Neural Network
CT	Computed Tomography
ECOG	Eastern Cooperative Oncology Group
GLCM	Gray Level Co-occurrence Matrix
GLRLM	Gray Level Run Length Matrix
GLSZM	Gray Level Size Zone Matrix
GLDM	Gray Level Dependence Matrix
GTV	Gross Tumor Volume
ICC	Intraclass Correlation Coefficient
IT	Induction Therapy
LASSO	Least Absolute Shrinkage and Selection Operator
LA	NSCLC-Locally Advanced Non-Small Cell Lung Cancer
MRI	Magnetic Resonance Imaging
GTDM	Neighborhood Gray Tone Difference Matrix
NSCLC	Non-Small Cell Lung Cancer
PET	Positron Emission Tomography
PERI	Peritumoral
PS	Performance Status
RECIST	Response Evaluation Criteria in Solid Tumors
Rad	score-Radiomic Score
ROI	Region of Interest
SVM	Support Vector Machine
TRIPOD	Transparent Reporting of a Multivariable Prediction Model for Individual Prognosis or Diagnosis
XGBoost	Extreme Gradient Boosting

Supplementary Information

The online version contains supplementary material available at https://doi.org/10.1186/s12885-025-13804-x .

Supplementary Material 1

Author contributions

F.C. and Z.J.G. contributed equally to this work. F.C., Z.C., and G.Y.W. performed data collection and radiomic feature extraction. F.P.L., Y.Y., and M.L. conducted image preprocessing and segmentation. J.M.H., T.T., and Z.G.X. carried out statistical analysis and model development. X.H.B., X.Y.Z., and Z.Z.Y. contributed to feature selection and machine learning modeling. Z.C. supervised the study, contributed to writing the manuscript, and secured funding. All authors reviewed and approved the final manuscript.

Funding

National Natural Science Foundation of China, No.82273572. Natural Science Foundation of Chongqing, CSTB2023NSCQ-MSX0059. Chengdu Longquanyi district health committee medical topic Program of Chengdu, WJKY2024010.

Data availability

Full datasets generated during and/or analyzed during the current study are available from the corresponding author on reasonable request. Additional data are available in the supplementary materials.

Declarations

Ethics approval and consent to participate

This study was approved by the Ethics Committee of Sichuan University West China Longquan Hospital (Approval No. IRB-C-F10/AF-KY-2024028) and conducted in accordance with the Declaration of Helsinki. Given that this is a retrospective analysis and all patient data were anonymized, the Ethics Committee waived the requirement for individual informed consent. Similarly, approval for the external validation cohort was obtained from the Ethics Committee of the Cancer Center of the Second Affiliated Hospital of Chongqing Medical University (Approval No. KY2024394). All data processing procedures adhered to relevant ethical standards and privacy protection regulations.

Consent for publication

Not applicable.

Competing interests

The authors declare no competing interests.

Author details

[1]Department of Cancer Center, The Second Affiliated Hospital of Chongqing Medical University, No. 288 Tianwen Road, Nan'an District, Chongqing 400010, China
[2]Department of Oncology and Hematology, The First People's Hospital of Longquanyi District, No. 669, Donglang Road, Chengdu 610100, China
[3]Chongqing Key Laboratory of Immunotherapy, Chongqing 400010, China

Received: 22 December 2024 / Accepted: 25 February 2025
Published online: 13 March 2025

References

1. Bray F, Laversanne M, Sung H, Ferlay J, Siegel RL, Soerjomataram I, Jemal A. Global cancer statistics 2022: GLOBOCAN estimates of incidence and mortality worldwide for 36 cancers in 185 countries. CA Cancer J Clin. 2024 May-Jun;74(3):229–263. https://doi.org/10.3322/caac.21834. Epub 2024 Apr 4. PMID: 38572751.
2. Li C, Lei S, Ding L, Xu Y, Wu X, Wang H, Zhang Z, Gao T, Zhang Y, Li L. Global burden and trends of lung cancer incidence and mortality. Chin Med J (Engl). 2023 Mar 28. https://doi.org/10.1097/CM9.0000000000002529. Epub ahead of print. PMID: 37027426.
3. Bravis V, Kaur A, Walkey HC, Godsland IF, Misra S, Bingley PJ, Williams AJK, Dunger DB, Dayan CM, Peakman M, Oliver NS, Johnston DG. ADDRESS-2 management committee, patient advocate group and investigators. Relationship between islet autoantibody status and the clinical characteristics of children and adults with incident type 1 diabetes in a UK cohort. BMJ Open. 2018;8(4):e020904. https://doi.org/10.1136/bmjopen-2017-020904. PMID: 29622578; PMCID: PMC5893930.
4. Miao D, Zhao J, Han Y, Zhou J, Li X, Zhang T, Li W, Xia Y. Management of locally advanced non-small cell lung cancer: state of the Art and future directions. Cancer Commun (Lond). 2024;44(1):23–46. Epub 2023 Nov 20. PMID: 37985191; PMCID: PMC10794016.
5. Ettinger DS, Wood DE, Aisner DL, Akerley W, Bauman JR, Bharat A, Bruno DS, Chang JY, Chirieac LR, D'Amico TA, Dilling TJ, Dowell J, Gettinger S, Gubens MA, Hegde A, Hennon M, Lackner RP, Lanuti M, Leal TA, Lin J, Loo BW Jr, Lovly CM, Martins RG, Massarelli E, Morgensztern D, Ng T, Otterson GA, Patel SP, Riely GJ, Schild SE, Shapiro TA, Singh AP, Stevenson J, Tam A, Yanagawa J, Yang SC, Gregory KM, Hughes M. NCCN Guidelines Insights: Non-Small Cell Lung Cancer, Version 2.2021. J Natl Compr Canc Netw. 2021;19(3):254–266. https://doi.org/10.6004/jnccn.2021.0013. PMID: 33668021.
6. Allemani C, Matsuda T, Di Carlo V, Harewood R, Matz M, Nikšić M, Bonaventure A, Valkov M, Johnson CJ, Estève J, Ogunbiyi OJ, Azevedo E, Silva G, Chen WQ, Eser S, Engholm G, Stiller CA, Monnereau A, Woods RR, Visser O, Lim GH, Aitken J, Weir HK, Coleman MP, CONCORD Working Group. Global surveillance of trends in cancer survival 2000-14 (CONCORD-3): analysis of individual records for 37 513 025 patients diagnosed with one of 18 cancers from 322 population-based registries in 71 countries. Lancet. 2018;391(10125):1023–75. https://doi.org/10.1016/S0140-6736(17)33326-3. Epub 2018 Jan 31. PMID: 29395269; PMCID: PMC5879496.
7. Renzulli M, Mottola M, Coppola F, Cocozza MA, Malavasi S, Cattabriga A, Vara G, Ravaioli M, Cescon M, Vasuri F, Golfieri R, Bevilacqua A. Automatically extracted machine learning features from preoperative CT to early predict microvascular invasion in HCC: the role of the zone of transition (ZOT). Cancers (Basel). 2022;14(7):1816. https://doi.org/10.3390/cancers14071816. PMID: 35406589; PMCID: PMC8997857.
8. Nikfar M, Mi H, Gong C, Kimko H, Popel AS. Quantifying intratumoral heterogeneity and immunoarchitecture generated In-Silico by a Spatial quantitative systems Pharmacology model. Cancers (Basel). 2023;15(10):2750. https://doi.org/10.3390/cancers15102750. PMID: 37345087; PMCID: PMC10216176.
9. Armani G, Madeddu D, Mazzaschi G, Bocchialini G, Sogni F, Frati C, Lorusso B, Falco A, Lagrasta CA, Cavalli S, Mangiaracina C, Vilella R, Becchi G, Gnetti L, Corradini E, Quaini E, Urbanek K, Goldoni M, Carbognani P, Ampollini L, Quaini F. Blood and lymphatic vessels contribute to the impact of the immune microenvironment on clinical outcome in non-small-cell lung cancer. Eur J Cardiothorac Surg. 2018;53(6):1205–1213. https://doi.org/10.1093/ejcts/ezx492. PMID: 29346540.
10. Guo M, Sun Y, Wang X, Wang Z, Yuan X, Chen X, Yuan X, Wang L. The MCIB model: A novel theory for describing the Spatial heterogeneity of the tumor microenvironment. Int J Mol Sci. 2024;25(19):10486. https://doi.org/10.3390/ijms251910486. PMID: 39408814; PMCID: PMC11476373.
11. Shimada Y, Ishii G, Hishida T, Yoshida J, Nishimura M, Nagai K. Extratumoral vascular invasion is a significant prognostic indicator and a predicting factor of distant metastasis in non-small cell lung cancer. J Thorac Oncol. 2010;5(7):970–5. https://doi.org/10.1097/JTO.0b013e3181dd1803. PMID: 20512073.
12. Zhang L, Yankelevitz DF, Henschke CI, Jirapatnakul AC, Reeves AP, Carter D. Zone of transition: a potential source of error in tumor volume Estimation. Radiology. 2010;256(2):633–9. https://doi.org/10.1148/radiol.10090924. PMID: 20656844; PMCID: PMC2909437.
13. Mottola M, Golfieri R, Bevilacqua A. The effectiveness of an adaptive method to analyse the transition between tumour and peritumour for answering two clinical questions in Cancer imaging. Sens (Basel). 2024;24(4):1156. https://doi.org/10.3390/s24041156. PMID: 38400314; PMCID: PMC10893370.
14. Moons KG, Altman DG, Reitsma JB, Ioannidis JP, Macaskill P, Steyerberg EW, Vickers AJ, Ransohoff DF, Collins GS. Transparent Reporting of a multivariable prediction model for Individual Prognosis or Diagnosis (TRIPOD): explanation and elaboration. Ann Intern Med. 2015;162(1):W1-73. https://doi.org/10.7326/M14-0698. PMID: 25560730.
15. Matschinske J, Alcaraz N, Benis A, Golebiewski M, Grimm DG, Heumos L, Kacprowski T, Lazareva O, List M, Louadi Z, Pauling JK, Pfeifer N, Röttger R, Schwämmle V, Sturm G, Traverso A, Van Steen K, de Freitas MV, Villalba Silva GC, Wee L, Wenke NK, Zanin M, Zolotareva O, Baumbach J, Blumenthal DB. The AIMe registry for artificial intelligence in biomedical research. Nat

Methods. 2021;18(10):1128–1131. https://doi.org/10.1038/s41592-021-01241-0. PMID: 34433960.
16. Schwartz LH, Litière S, de Vries E, Ford R, Gwyther S, Mandrekar S, Shankar L, Bogaerts J, Chen A, Dancey J, Hayes W, Hodi FS, Hoekstra OS, Huang EP, Lin N, Liu Y, Therasse P, Wolchok JD, Seymour L. RECIST 1.1-Update and clarification: from the RECIST committee. Eur J Cancer. 2016;62:132–7. Epub 2016 May 14. PMID: 27189322; PMCID: PMC5737828.
17. Whybra P, Zwanenburg A, Andrearczyk V, Schaer R, Apte AP, Ayotte A, Baheti B, Bakas S, Bettinelli A, Boellaard R, Boldrini L, Buvat I, Cook GJR, Dietsche F, Dinapoli N, Gabryś HS, Goh V, Guckenberger M, Hatt M, Hosseinzadeh M, Iyer A, Lenkowicz J, Loutfi MAL, Löck S, Marturano F, Morin O, Nioche C, Orlhac F, Pati S, Rahmim A, Rezaeijo SM, Rookyard CG, Salmanpour MR, Schindele A, Shiri I, Spezi E, Tanadini-Lang S, Tixier F, Upadhaya T, Valentini V, van Griethuysen JJM, Yousefirizi F, Zaidi H, Müller H, Vallières M, Depeursinge A. The image biomarker standardization initiative: standardized convolutional filters for reproducible radiomics and enhanced clinical insights. Radiology. 2024;310(2):e231319. https://doi.org/10.1148/radiol.231319. PMID: 38319168; PMCID: PMC10902595.
18. Demircioğlu A. The effect of feature normalization methods in radiomics. Insights Imaging. 2024;15(1):2. https://doi.org/10.1186/s13244-023-01575-7. PMID: 38185786; PMCID: PMC10772134.
19. Spearman's rank correlation coefficient. BMJ. 2018;362:k4131. https://doi.org/10.1136/bmj.k4131. Erratum for: BMJ. 2014;349:g7327. https://doi.org/10.1136/bmj.g7327. PMID: 30270200.
20. Hu Y, Xie C, Yang H, Ho JWK, Wen J, Han L, Chiu KWH, Fu J, Vardhanabhuti V. Assessment of intratumoral and peritumoral computed tomography radiomics for predicting pathological complete response to neoadjuvant chemoradiation in patients with esophageal squamous cell carcinoma. JAMA Netw Open. 2020;3(9):e2015927. https://doi.org/10.1001/jamanetworkopen.2020.15927. PMID: 32910196; PMCID: PMC7489831.
21. Chen X, Yang Z, Yang J, Liao Y, Pang P, Fan W, Chen X. Radiomics analysis of contrast-enhanced CT predicts lymphovascular invasion and disease outcome in gastric cancer: a preliminary study. Cancer Imaging. 2020;20(1):24. https://doi.org/10.1186/s40644-020-00302-5. PMID: 32248822; PMCID: PMC7132895.
22. Surjanovic N, Lockhart RA, Loughin TM. A generalized Hosmer-Lemeshow goodness-of-fit test for a family of generalized linear models. Test (Madr). 2024;33(2):589–608. https://doi.org/10.1007/s11749-023-00912-8. Epub 2023 Dec 19. PMID: 38868722; PMCID: PMC11164741.
23. Van Calster B, Wynants L, Verbeek JFM, Verbakel JY, Christodoulou E, Vickers AJ, Roobol MJ, Steyerberg EW. Reporting and interpreting decision curve analysis: A guide for investigators. Eur Urol. 2018;74(6):796–804. https://doi.org/10.1016/j.eururo.2018.08.038. Epub 2018 Sep 19. PMID: 30241973; PMCID: PMC6261531.
24. Jiang Y, Wang H, Wu J, Chen C, Yuan Q, Huang W, Li T, Xi S, Hu Y, Zhou Z, Xu Y, Li G, Li R. Noninvasive imaging evaluation of tumor immune microenvironment to predict outcomes in gastric cancer. Ann Oncol. 2020;31(6):760–768. https://doi.org/10.1016/j.annonc.2020.03.295. Epub 2020 Mar 30. Erratum in: Ann Oncol. 2021;32(4):578. https://doi.org/10.1016/j.annonc.2021.01.064. PMID: 32240794.
25. Walsh LA, Quail DF. Decoding the tumor microenvironment with Spatial technologies. Nat Immunol. 2023;24(12):1982–93. https://doi.org/10.1038/s41590-023-01678-9. Epub 2023 Nov 27. PMID: 38012408.
26. Chang R, Qi S, Zuo Y, Yue Y, Zhang X, Guan Y, Qian W. Predicting chemotherapy response in non-small-cell lung cancer via computed tomography radiomic features: peritumoral, intratumoral, or combined? Front Oncol. 2022;12:915835. https://doi.org/10.3389/fonc.2022.915835. PMID: 36003781; PMCID: PMC9393703.
27. Chen Z, Yi G, Li X, Yi B, Bao X, Zhang Y, Zhang X, Yang Z, Guo Z. Predicting radiation pneumonitis in lung cancer using machine learning and multimodal features: a systematic review and meta-analysis of diagnostic accuracy. BMC Cancer. 2024;24(1):1355. https://doi.org/10.1186/s12885-024-13098-5. PMID: 39501204; PMCID: PMC11539622.
28. Zou Z, Li J, Ji X, Wang T, Chen Q, Liu Z, Ji S. Naples prognostic score as an independent predictor of survival outcomes for resected locally advanced Non-Small cell lung Cancer patients after neoadjuvant treatment. J Inflamm Res. 2023;16:793–807. PMID: 36860794; PMCID: PMC9969868.
29. Zhou Q, Chen M, Jiang O, Pan Y, Hu D, Lin Q, Wu G, Cui J, Chang J, Cheng Y, Huang C, Liu A, Yang N, Gong Y, Zhu C, Ma Z, Fang J, Chen G, Zhao J, Shi A, Lin Y, Li G, Liu Y, Wang D, Wu R, Xu X, Shi J, Liu Z, Cui N, Wang J, Wang Q, Zhang R, Yang J, Wu YL. Sugemalimab versus placebo after concurrent or sequential chemoradiotherapy in patients with locally advanced, unresectable, stage III non-small-cell lung cancer in China (GEMSTONE-301): interim results of a randomised, double-blind, multicentre, phase 3 trial. Lancet Oncol. 2022;23(2):209–19. https://doi.org/10.1016/S1470-2045(21)00630-6. Epub 2022 Jan 14. PMID: 35038429.
30. Arslan D, Bozcuk H, Gunduz S, Tural D, Tattli AM, Uysal M, Goksu SS, Bassorgun Cİ, Koral L, Coskun HS, Ozdogan M, Savas B. Survival results and prognostic factors in T4 N0-3 non-small cell lung cancer patients according to the AJCC 7th edition staging system. Asian Pac J Cancer Prev. 2014;15(6):2465-72. https://doi.org/10.7314/apjcp.2014.15.6.2465. PMID: 24761848.
31. Mayerhoefer ME, Materka A, Langs G, Häggström I, Szczypiński P, Gibbs P, Cook G. Introduction to radiomics. J Nucl Med. 2020;61(4):488–95. https://doi.org/10.2967/jnumed.118.222893. Epub 2020 Feb 14. PMID: 32060219; PMCID: PMC9374044.
32. Crowson CS, Atkinson EJ, Therneau TM. Assessing calibration of prognostic risk scores. Stat Methods Med Res. 2016;25(4):1692– 706. https://doi.org/10.1177/0962280213497434. Epub 2013 Jul 30. Erratum in: Stat Methods Med Res. 2017;26(4):1992–1993. https://doi.org/10.1177/0962280217719818. PMID: 23907781; PMCID: PMC3933449.
33. Staffa SJ, Zurakowski D. Statistical Development and Validation of Clinical Prediction Models. Anesthesiology. 2021;135(3):396–405. https://doi.org/10.1097/ALN.0000000000003871. PMID: 34330146.
34. Mjahad A, Saban M, Azarmdel H, Rosado-Muñoz A. Efficient extraction of deep image features using a convolutional neural network (CNN) for detecting ventricular fibrillation and tachycardia. J Imaging. 2023;9(9):190. https://doi.org/10.3390/jimaging9090190. PMID: 37754954; PMCID: PMC10532022.
35. Amin MN, Rushdi MA, Marzaban RN, Yosry A, Kim K, Mahmoud AM. Wavelet-based Computationally-Efficient Computer-Aided characterization of liver steatosis using conventional B-mode ultrasound images. Biomed Signal Process Control. 2019;52:84–96. https://doi.org/10.1016/j.bspc.2019.03.010. Epub 2019 Apr 5. PMID: 31983924; PMCID: PMC6980471.
36. Kang W, Qiu X, Luo Y, Luo J, Liu Y, Xi J, Li X, Yang Z. Application of radiomics-based multiomics combinations in the tumor microenvironment and cancer prognosis. J Transl Med. 2023;21(1):598. https://doi.org/10.1186/s12967-023-04437-4. PMID: 37674169; PMCID: PMC10481579.

Publisher's note